Molecular Crystals and Liquid Crystals Science and Technology. Section A. Molecular Crystals and Liquid Crystals

Publication details, including instructions for authors and subscription information:
http://www.tandfonline.com/loi/gmcl19

Numerical Modelling of Multi-Dimensional Liquid Crystal Optics: Finite-Difference Time-Domain Method

Emmanouil E. Kriezis [a] & Steve J. Elston [a]

[a] University of Oxford, Department of Engineering Science Parks Road, Oxford, OX1 3PJ, United Kingdom

Version of record first published: 24 Sep 2006

To cite this article: Emmanouil E. Kriezis & Steve J. Elston (2001): Numerical Modelling of Multi-Dimensional Liquid Crystal Optics: Finite-Difference Time-Domain Method, Molecular Crystals and Liquid Crystals Science and Technology. Section A. Molecular Crystals and Liquid Crystals, 359:1, 289-299

To link to this article: http://dx.doi.org/10.1080/10587250108035588

Mol. Cryst. and Liq. Cryst., 2001, Vol. 359, pp. 289-299
Reprints available directly from the publisher
Photocopying permitted by license only

Numerical Modelling of Multi-Dimensional Liquid Crystal Optics: Finite-Difference Time-Domain Method

EMMANOUIL E. KRIEZIS and STEVE J. ELSTON

University of Oxford, Department of Engineering Science Parks Road, Oxford OX1 3PJ, United Kingdom

Light wave propagation within complex liquid crystal structures is undertaken by the FDTD method, a purely numerical method that explicitly solves Maxwell's equations in space and time. A specific FDTD arrangement suitable for liquid crystal applications is described, allowing for efficient space termination, oblique angles of illumination, and correct phasor representation. Two application examples are considered: a two-domain twisted pixel formed by two oppositely twisted sub-domains, and a helical ferroelectric liquid crystal material. In each case comparison is also made with the optical prediction obtained by the Berreman method.

Keywords: Finite-Difference Time-Domain Method; LC Optics

INTRODUCTION

Modelling of liquid crystal optics is currently dominated by the application of matrix-type solvers, and in particular the Jones 2×2 method for simpler cases, and the Berreman 4×4 method [1] for more demanding ones. All matrix-type solvers are built on the stratified medium approach, which limits the liquid crystal spatial variation to the direction normal to the supporting surfaces. This approach may be sufficient when each individual pixel spans the extent of many optical

wavelengths, and is further characterised by a slow variation along the transverse directions. However in a significant number of currently evolving LC devices the stratified medium approach seems to be under dispute. Examples include small-sized pixels for head-mounted displays, pixel edges, multi-domain liquid crystal displays, defects, domain-walls in ferroelectric LC and zenithal bistable nematic cells. This has resulted in interest in applying rigorous numerical methods capable of coping with LC variation in more than one dimension.

Finite-Difference Time-Domain (FDTD) methods represent the most general approach to direct solution of Maxwell's equations, both in space and time. Here we discuss a FDTD arrangement that overcomes some of the former difficulties associated with initial attempts at FDTD application in LC devices [2-4].

Example applications are presented for practical twisted/tilted nematic devices and ferroelectrics, corresponding to cases violating the stratified medium approach. As a first example we examine a multi-domain pixel structure, as proposed in [5] to improve the field of view. A second example examines the interaction of light with the helix present in ferroelectric LC devices. The results are assessed by comparing them with the prediction of the 4×4 Berreman method and identifying the breakdown point of the matrix solvers. Conclusions are drawn as to further promising applicability of the FDTD method to LC optics.

FINITE-DIFFERENCE TIME-DOMAIN METHOD FOR LIQUID CRYSTAL DEVICES

The mathematical formulation is based on the solution of Maxwell's equation for an inhomogeneous anisotropic medium in 2-D. Therefore, the electric and magnetic field should satisfy the coupled curl equations:

$$\tilde{\varepsilon}(\mathbf{r})\frac{\partial \mathbf{E}(\mathbf{r})}{\partial t} = \nabla \times \mathbf{H}(\mathbf{r}) \tag{1}$$

$$\mu_0 \frac{\partial \mathbf{H}(\mathbf{r})}{\partial t} = -\nabla \times \mathbf{E}(\mathbf{r}) \tag{2}$$

In equations (1) and (2) the vector $\mathbf{r} = x\hat{\mathbf{x}} + z\hat{\mathbf{z}}$ is allowed to vary in the xOz plane, as the problem is treated as a two-dimensional one.

Equations (1) and (2) are discretised in space and time by central finite differences. In space a staggered grid consisting of Yee cells [6] is used, as shown in figure 1. In time a leap frog scheme is employed assigning electric and magnetic field values at time instances $\Delta t/2$ apart, as suggested in [6]. Finally, a fully explicit finite difference scheme is developed, allowing for correct and efficient time marching of the coupled fields involved.

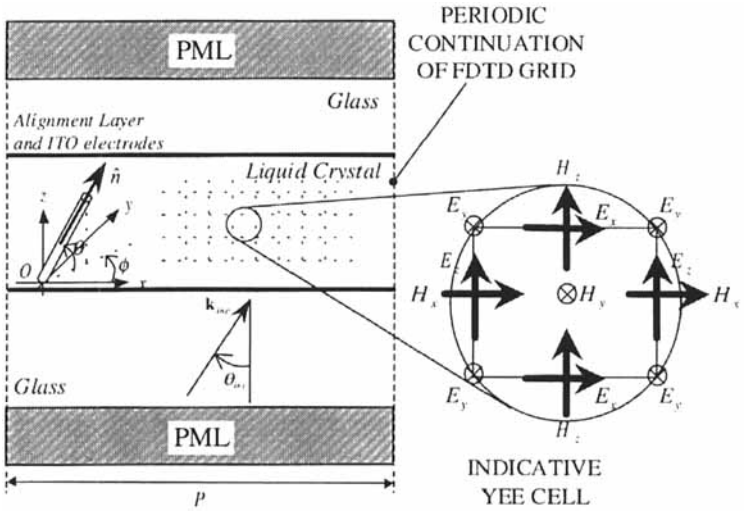

FIGURE 1 FDTD computational space layout for liquid crystal applications. The rod-like molecules are oriented according to the tilt (θ) and twist (ϕ) angles. An indicative variant of Yee's cell in 2-D is also shown.

The proposed arrangement (figure 1) encloses the computational space between two Perfectly Matched Layer (PML) [7] slabs, along the cell normal direction to provide an efficient reflection-free termination. PML slabs have been introduced by Berenger, and now are widely used

as they outperform all previous absorbing boundary conditions used for grid termination. The grid termination is completed by enforcing Periodic Boundary Conditions (PBC) along the transverse direction. This completely avoids spurious diffracted components when launching the illuminating field, and furthermore, provides a sound basis for accurate implementation of obliquely incident waves. The oblique incidence is implemented in conjunction with the PBC by using a dual-time excitation technique, where two spatially identical but otherwise 90° out of phase impinging waves are used [8]. Under this approach the incident electric field is written as:

$$\mathbf{E}'_{inc}(x,z,t) = \mathbf{E}_0 \cos(\omega t - k_{inc} \sin\theta_{inc} x - k_{inc} \cos\theta_{inc} z) \quad (3)$$

$$\mathbf{E}''_{inc}(x,z,t) = \mathbf{E}_0 \sin(\omega t - k_{inc} \sin\theta_{inc} x - k_{inc} \cos\theta_{inc} z) \quad (4)$$

The response to the incident plane wave of equation (3) is $(\mathbf{E}', \mathbf{H}')$, whereas the response to the wave of equation (4) is $(\mathbf{E}'', \mathbf{H}'')$. Periodicity is enforced in the spectral domain, an intuitively expected, by the following operations, which are given for the magnetic field:

$$\mathbf{H}'(x+P,z,t) = \mathrm{Re}\{[\mathbf{H}'(x,z,t) + j\mathbf{H}''(x,z,t)]\exp(-jk_{inc}\sin\theta_{inc}P)\} \quad (5)$$

$$\mathbf{H}''(x+P,z,t) = \mathrm{Im}\{[\mathbf{H}'(x,z,t) + j\mathbf{H}''(x,z,t)]\exp(-jk_{inc}\sin\theta_{inc}P)\} \quad (6)$$

The quantity P is the spatial period along the x-direction. Similar expressions hold for all other field components involved.

Dual-time excitation also provides an efficient and robust way for consistent extraction of magnitude and phase information from the harmonic fields propagating within the LC device, which is of significant importance.

NUMERICAL SIMULATIONS AND DISCUSSION

Modelling of Multi-Domain Liquid Crystal Displays

As a first numerical application we shall consider light propagation within a multi-domain twisted nematic pixel for wide-viewing angle displays [5]. A single pixel consists of two different twisted domains with opposite sense of rotation. The geometrical

characteristics of a single pixel, together with the electrodes print and the aligning directions are schematically shown in figure 2. This geometrical configuration results in a complicated director profile with significant transverse variation as a consequence of the oppositely imposed alignments. Therefore light wave propagation should be studied by the application of the FDTD method, as the standard Berreman method [1] might not be adequate.

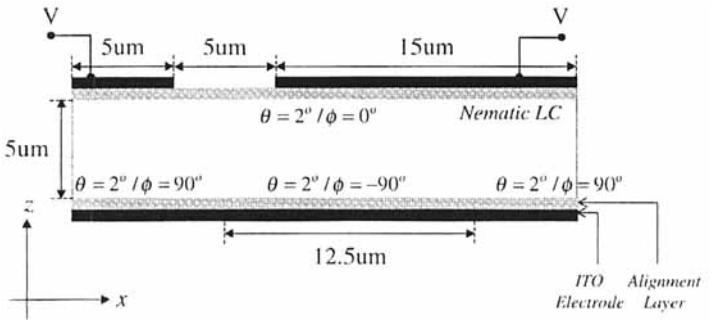

FIGURE 2 Two-domain pixel geometry with oppositely twisted sub-domains. The block shown is assumed to be repeated periodically along the transverse direction. The LC material elastic constants are: $K_{11} = 12.5pN$ $K_{22} = 7.3pN$ $K_{33} = 17.9pN$. The static dielectric constants are $\varepsilon_{\perp} = 4.1, \varepsilon_{//} = 14.1$.

All calculations have been performed by both methods (FDTD method and Berreman method) on a matching grid. In practise, a grid consisting of 1250×250 Yee cells was used to model the liquid crystal material. This is equivalent to $\delta x = \delta z = 20nm$, and a temporal step of $\delta t = 4.5 \times 10^{-17} s$ was used in conjunction with this to ensure stability. The actual grid used in the FDTD calculations was extended along the z-direction to accommodate some more Yee cells for the surrounding glass medium and the necessary PML slabs. 20-point thick PML slabs were used, having a parabolic conductivity profile and a maximum theoretical reflectivity of 10^{-5}. Their performance was found to be very

satisfactory. In all calculations the ordinary refractive index was set to $n_o = 1.5$, the extra-ordinary index was $n_e = 1.6$, and the supporting glass index was $n_{glass} = 1.5$. For simplicity the ITO layer was not considered in the optical calculations.

The normalised transmitted optical intensity between crossed ideal polarising elements is shown in figure 3, for the case of normal incidence. The input polariser is oriented along $\phi_{in} = 90^o$ and exit polariser is along $\phi_{out} = 0^o$. A free space wavelength of $\lambda = 650nm$ has been considered and light is assumed to propagate towards the $+\hat{z}$ direction. Figure 3a illustrates the case with no applied voltage, whereas, figure 3b corresponds to a switched state with impressed voltage $V = 2Volts$. The agreement is quite satisfactory in the case of figure 3a, as the propagation mechanism is mainly due to the polarisation rotation caused by the presence of the twist. However, in the case of figure 3b the deviation is more significant, as the application of the static field results in a steeper director profile. In particular, the Berreman method fails to predict the correct influence of the disinclination line which contributes to the peak found on the left part of both curves of figure 3b. It should be noted that the FDTD prediction exhibits a high frequency ringing, which is not seen in the Berreman solution. This originates from scattering effects caused by the different LC alignment directions

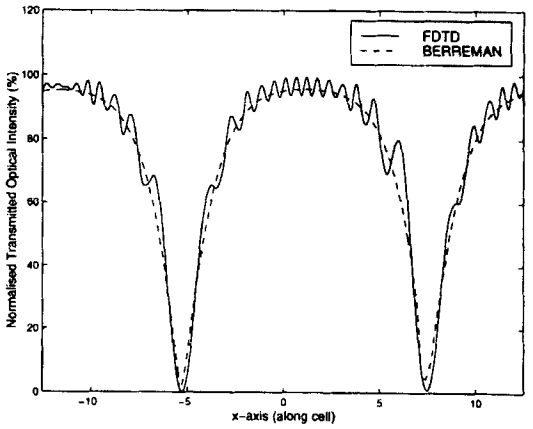

(a)

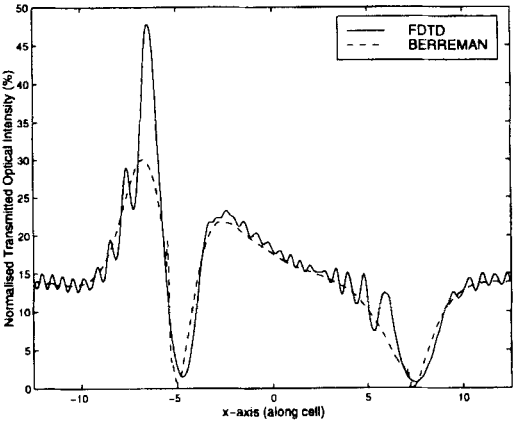

(b)

FIGURE 3 Normalised transmitted optical intensity over the extent of a single pixel (period) for the case of normal incidence. (a) $V = 0\,Volts$. (b) $V = 2\,Volts$.

present in the sample. These scattered light components interfere, leading to the ringing. The same effects are not observed if the LC region in figure 2 is occupied by the usual TN mono-domain.

Figure 4 concentrates on the case of oblique incidence with $\theta_{inc} = 30^{o}$. All parameters and the orientation of the polarisers are left unchanged. When illuminating off-axis differences are even more pronounced. Although the Berreman method roughly predicts the transmitted intensity shape, it fails to correctly predict the location of the various features caused by the presence of the disinclination line or the boundary between regions with different alignment direction. This is intuitively expected for the case of oblique illumination and it accounts for fields crossing the feature at different positions. In the case of the Berreman method the 2-D director profile is decomposed into a number of stratified profiles (stacks), and each stack is treated completely independent of all others as if it extends to infinity. As a result, some important information is lost. Also the results shown in figure 4 include all interference effects arising from multiple scattering/diffraction mechanisms, these lead to the high spatial frequency ringing described above.

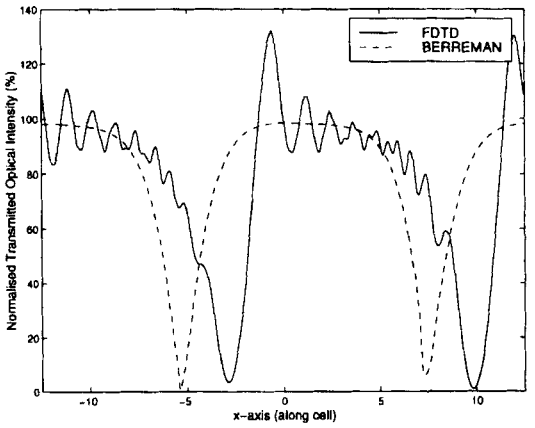

(a)

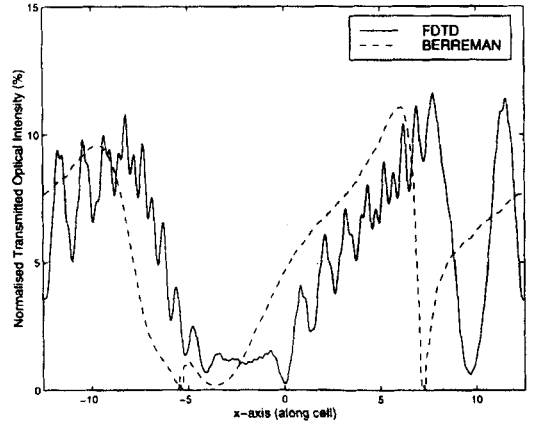

(b)

FIGURE 4 Normalised transmitted optical intensity over the extent of a single pixel (period) for the case of oblique incidence $\theta_{inc} = 30^{o}$ (a) $V = 0\,Volts$. (b) $V = 2\,Volts$.

Light Propagation in Helical Ferroelectric Liquid Crystals

As a second application we concentrate on light wave propagation within a chiral ferroelectric liquid crystal medium. In particular, propagation of light perpendicular to the helix axis is studied (figure 5). As this case possesses transverse only variation (along the x-direction), we expect agreement between the FDTD method and the Berreman method in the case of long (compared to the optical wavelength) helical pitch. If the helical pitch is decreased, the difference between the two methods will be more pronounced as the Berreman method ignores all associated diffractive phenomena, which are now important. Furthermore, the inherent periodicity of the helical structure fits into the framework of the periodic continuation used for the FDTD grid.

Three sets of calculations have been performed by both methods. In all three cases the sample thickness was kept constant at $5\mu m$. The transverse window dimension was set equal to one helical pitch (2π angle variation measured in the smectic cone), and the helical pitch was varied ($5\mu m, 10\mu m, 20\mu m$). The normalised transmitted optical intensity versus the transverse distance normalised to the helical pitch is plotted in figure 6, for a free space wavelength of $\lambda = 650nm$. The spatial and temporal discretisation from the previous application have been retained ($\delta x = \delta z = 20nm, \delta t = 4.5\times10^{-17} s$). PML slabs with analogous characteristics to the previous example have also been utilised. A smectic cone angle of $\Theta = 20^{o}$ has been used.

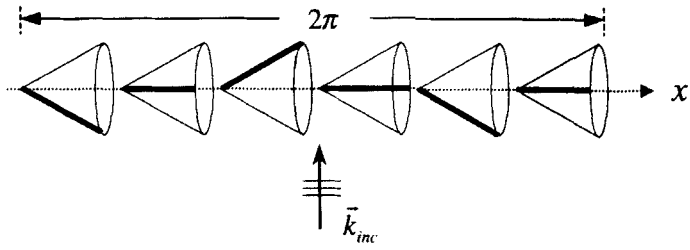

FIGURE 5 Single helical pitch of a chiral ferroelectric liquid crystal material corresponding to 2π variation along the smectic cone.

The polarisers are oriented along the directions $\phi_{in} = 90^o$ and $\phi_{out} = 0^o$. It is apparent that the curve predicted by the Berreman method coincides in all three cases as the transverse rate of change is not taken into consideration. The FDTD prediction deviates significantly in the regime of small helical pitches (which might more likely be encountered in practical applications), whereas tends to the Berreman prediction for sufficiently long helical pitches.

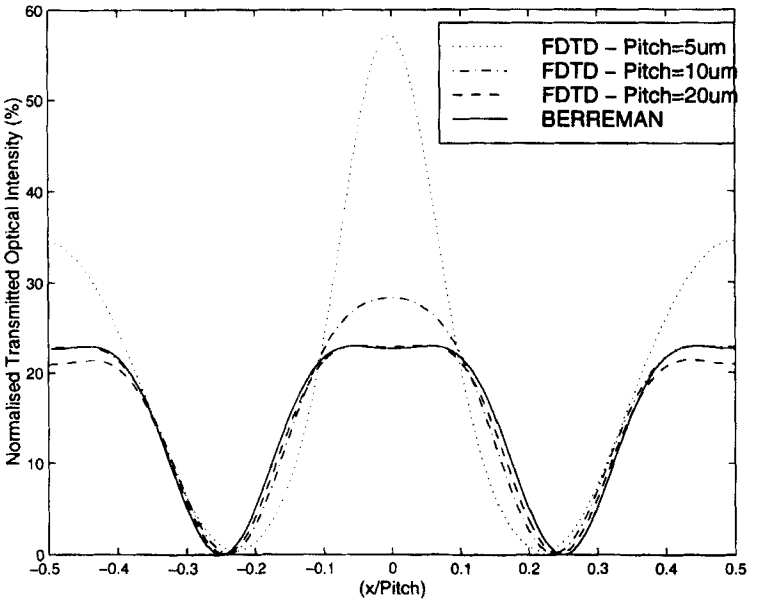

FIGURE 6 Normalised transmitted optical intensity over the extent of a complete helical pitch. Three different pitches are illustrated: $5\mu m, 10\mu m, 20\mu m$. The Berreman curve remains exactly the same in all three cases.

CONCLUSIONS

A consistent FDTD method in 2-D for liquid crystal light propagation in applications has been presented. The method is capable of solving complicated geometrical configurations corresponding to cases where the application of matrix-type solvers is not fully justified. Two different applications from nematics and ferroelectrics were demonstrated. The FDTD method appears to be a very robust technique, which leads to significant improvement over the stratified medium approach for complex director structures.

Acknowledgements
The authors wish to acknowledge the financial support of the EPSRC. Furthermore, they wish also to acknowledge Sharp Laboratories of Europe (SLE Ltd.) for their help.

References

[1] D. W. Berreman, *J. Opt. Soc. Am.*, **62,** pp. 502–510, (1972).
[2] B. Witzigmann, P. Regli, and W. Fichtner, *J. Opt. Soc. Am. A.*, **15,** pp. 753–757, (1998).
[3] C. M. Titus, P. J. Bos, and J. R. Kelly, *SID 99 DIGEST,* pp. 624–627, (1999).
[4] E. E. Kriezis, and S. J. Elston, *Optics Comm.*, **165,** pp. 99–105, (1999).
[5] M. Schadt, H. Seiberle, and A. Schuster, *Nature*, **381,** pp. 212–215, (1996).
[6] K. Yee, *IEEE Trans. Antennas Propag.*, **14,** pp. 302–307, (1966).
[7] J. P. Berenger, *J. of Computational Physics*, **114,** pp. 185–200, (1994).
[8] P. Harms, R. Mittra, and W. Ko, *IEEE Trans. Antennas Propag.*, **42,** pp. 1317–1324, (1994).